

# Inner-shell ionization by ultrarelativistic electrons Inner-shell ionization by ultrarelativistic electrons

|                              |   |
|------------------------------|---|
| 著者                           | 石井 慶造   |
| journal or publication title | Physical review. A  |
| volume                       | 15  |
| number                       | 3   |
| page range                   | 906-913   |
| year                         | 1977  |
| URL                          | <a href="http://hdl.handle.net/10097/35214">http://hdl.handle.net/10097/35214</a> |

doi: 10.1103/PhysRevA.15.906

## Inner-shell ionization by ultrarelativistic electrons

K. Ishii, M. Kamiya, K. Sera, and S. Morita

*Department of Physics, Tohoku University, Sendai, Japan*

H. Tawara

*Nuclear Engineering Department, Kyushu University, Fukuoka, Japan*

M. Oyamada

*Laboratory of Nuclear Science, Tohoku University, Sendai, Japan*

T. C. Chu\*

*Department of Chemistry, Tohoku University, Sendai, Japan*

(Received 7 July 1976; revised manuscript received 4 October 1976)

We have measured  $K$ -shell ionization cross sections by electron impact for 19 elements with atomic number in the range  $Z = 13$ –92,  $L$ - and  $M$ -shell ionization cross sections for nine and two heavier elements, respectively, in the energy range 70–270 MeV. The results on the  $K$ -shell ionization were compared with the predictions from the revised Kolbenstvedt theory and the plane-wave Born approximation calculation by Davidović and Moiseiwitsch, and good agreements were obtained. The  $L$ - and  $M$ -shell ionization cross sections were also compared with the predictions from the Kolbenstvedt theory using photoeffect cross sections for these shells and good agreements were obtained, although there is some ambiguity in the photoeffect cross section used in the estimation. The  $K$ -shell ionization cross sections, together with other experimental results, were represented in a good scaled form based on the revised Kolbenstvedt theory.

### I. INTRODUCTION

Experimental studies on inner-shell ionization by electron impact in a region above several MeV are still scarce. In 1970, Middleman *et al.*<sup>1</sup> measured the  $K$ -shell ionization cross sections of eight elements with atomic number in the range  $Z = 29$ –83 and also  $L$ -shell ionization cross sections of four higher- $Z$  elements over the incident energy range 150–900 MeV using the Stanford linear accelerator Mark III; they showed that the experimental results are in good agreement with the revised Kolbenstvedt theory<sup>2</sup> of approximate virtual photon method.

Recently Dangerfield and Spicer<sup>3</sup> measured the  $K$ -shell ionization cross sections of Ni, Ag, and Au with incident electrons over the energy range 3–30 MeV using external beams from a betatron and an NaI scintillation counter. Their results are somewhat inconsistent with other experimental results. They estimated the ionization cross sections from the Kolbenstvedt theory by taking photoeffect cross sections of Stobbe<sup>4</sup> and of Schmickley and Pratt<sup>5</sup> and pointed out that there is no theory which can reproduce the experimental results well over the whole relativistic energy range 0.1–900 MeV and also that the lack of evidence on the predicted density effect<sup>6</sup> is puzzling. Genz *et al.*<sup>7</sup> recently reported experimental results on  $K$ -shell ionization cross sections in the energy region 20–60 MeV.

We recently measured the  $K$ -shell ionization cross sections for several elements over the energy range 70–270 MeV and compared the results with the theoretical predictions in scaled representations.<sup>8</sup>

Here the measurements are extended to other elements and to  $L$ - and  $M$ -shell ionizations, and the results on  $K$ -shell ionizations, together with the other experimental results, are compared with the theoretical predictions from the revised Kolbenstvedt theory and from the plane-wave Born approximation (PWBA) theory of Davidović and Moiseiwitsch<sup>9</sup> in some scaled representations. The Kolbenstvedt theory is also applied to  $L$ - and  $M$ -shell ionizations by using the photoeffect cross sections for these shells.

### II. EXPERIMENT

Electron beams were accelerated by the 300-MeV linear accelerator of Tohoku University. The general experimental setup is shown in Fig. 1. Since this accelerator produces 300 pulses per sec of 3  $\mu$ sec width, the pile-up effect is a serious problem in this measurement. In order to minimize this effect and background radiation, the beam current was measured with a secondary emission monitor (SEM) instead of a Faraday cup and the detector was set outside of the scattering chamber of 442 mm diameter at a backward direction of 150° to the beam and the beam current kept below

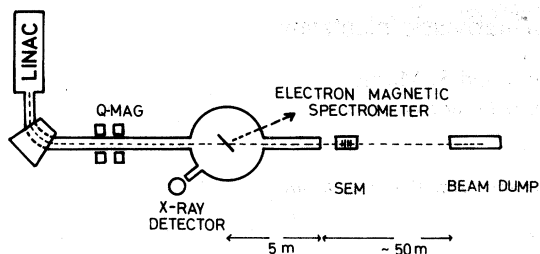


FIG. 1. Experimental arrangement. SEM is a secondary emission monitor.

several nanoamperes, corresponding to counting rates below 10 counts/sec. Elastically scattered electrons were also measured with the use of a magnetic spectrograph to monitor the beam current and to estimate the target thickness. A detector of Si(Li) or pure Ge was surrounded by lead blocks of about 10 cm thickness. The former detector was an Ortec with 205 eV energy resolution at 6 keV and was used for measurements of lower-energy x rays. The pure-Ge detector (Gamma-TEC) had an energy resolution of 180 eV at 6 keV and was used for higher-energy x rays. The efficiency curve for the Si(Li) detector measured with standard radioactive sources of  $^{241}\text{Am}$  and  $^{57}\text{Co}$  in our previous works<sup>10</sup> was used. The efficiency for the pure-Ge detector was measured by the same procedures as for the Si(Li) detector, and it was ascertained that the efficiency curves for these two detectors give consistent x-ray production cross sections in the overlapping energy region.

The targets of Mo, Pd, Sm, and Ho were prepared by vacuum evaporation on 4- $\mu\text{m}$  Mylar foils, and those of Cu, Zn, Se, Y, In, Sn, Pb, and Bi were on aluminum foils. The Ca and Ba targets were prepared by evaporating on Al foils and were covered with aluminum to avoid oxidation. Targets of Al, Si, and Au were self-supporting. A VYNS foil was used as the Cl target. The U target was prepared by electro-spraying of a solution of uranylacetate  $[(\text{CH}_3\text{COO})_2\text{UO}_2 \cdot 2\text{H}_2\text{O}]$  onto an 100- $\mu\text{g}/\text{cm}^2$  Al foil. The thickness of targets was measured by elastic scattering of electrons and 3-MeV protons from a Van de Graaff generator. The targets used are summarized in Table I.

Some of the spectra obtained are shown in Figs. 2(a)–2(c), which show sufficiently low and flat backgrounds. After subtracting the background, the counts of detected x rays were corrected for absorption in the target, in the window of the target chamber of a 10- $\mu\text{m}$ -thick Mylar foil and, in the 15.5-mm air path. The solid angle subtended by the detector was determined from the geometry.  $K$ -shell ionization cross sections were estimated

TABLE I. Targets used.

| Target atomic no. | X rays measured | Thickness ( $\mu\text{g}/\text{cm}^2$ ) |
|-------------------|-----------------|---|
| $^{13}\text{Al}$  | $K$             | 64.2                                    |
| $^{14}\text{Si}$  | $K$             | 363                                     |
| $^{17}\text{Cl}$  | $K$             | 36.0                                    |
| $^{20}\text{Ca}$  | $K$             | 73.1                                    |
| $^{29}\text{Cu}$  | $K$             | 45.6                                    |
| $^{30}\text{Zn}$  | $K$             | 276                                     |
| $^{34}\text{Se}$  | $K$             | 259                                     |
| $^{39}\text{Y}$   | $K$             | 133                                     |
| $^{42}\text{Mo}$  | $K$             | 454                                     |
| $^{46}\text{Pd}$  | $L$             | 27.8                                    |
| $^{49}\text{In}$  | $K$ and $L$     | 1183                                    |
| $^{50}\text{Sn}$  | $K$ and $L$     | 392                                     |
| $^{56}\text{Ba}$  | $K$ and $L$     | 193                                     |
| $^{62}\text{Sm}$  | $K$             | 299                                     |
| $^{67}\text{Ho}$  | $K$ and $L$     | 258                                     |
| $^{79}\text{Au}$  | $K$ and $L$     | 1280                                    |
| $^{82}\text{Pb}$  | $K, L$ and $M$  | 414                                     |
| $^{83}\text{Bi}$  | $K, L$ and $M$  | 235                                     |
| $^{92}\text{U}$   | $K$ and $L$     | 228                                     |

using the values of fluorescence yield shown in Table III.IV of a review article of Bambyneck *et al.*<sup>11</sup> as the selected “most reliable” experimental values or the fitted values, which are shown in Table II. The  $L$ -shell ionization cross sections were obtained from the mean fluorescence yield for  $L$ -shell  $\bar{\omega}_L$ , which is defined by

$$\bar{\omega}_L = \frac{\omega_1^{\text{eff}}/I_1 + \omega_2^{\text{eff}}/I_2 + 2\omega_3^{\text{eff}}/I_3}{1/I_1 + 1/I_2 + 2/I_3}, \quad (1)$$

where  $I_i$  is the ionization energy of the  $i$ th subshell and

$$\omega_1^{\text{eff}} = \omega_1 + f_{12}\omega_2 + (f_{13} + f_{12}f_{23})\omega_3,$$

$$\omega_2^{\text{eff}} = \omega_2 + f_{23}\omega_3,$$

$$\omega_3^{\text{eff}} = \omega_3,$$

the  $\omega_i$  being the fluorescence yield for the  $i$ th subshell and the  $f_{ij}$  the Coster-Kronig transition coefficient between the  $i$ th and  $j$ th subshells. The values of these quantities were taken from Table IV.XV of Bambyneck *et al.*<sup>11</sup> The mean fluorescence yields for  $M$ -shell were also from Table V.III of that article.

### III. RESULTS AND DISCUSSION

The  $K$ -,  $L$ -, and  $M$ -shell ionization cross sections thus obtained, together with those of our previous measurements,<sup>8</sup> are shown in Tables II, III, and IV, respectively. Overall errors of the  $K$ -shell ionization cross sections are estimated to be 15%, except for 40% for lighter elements—

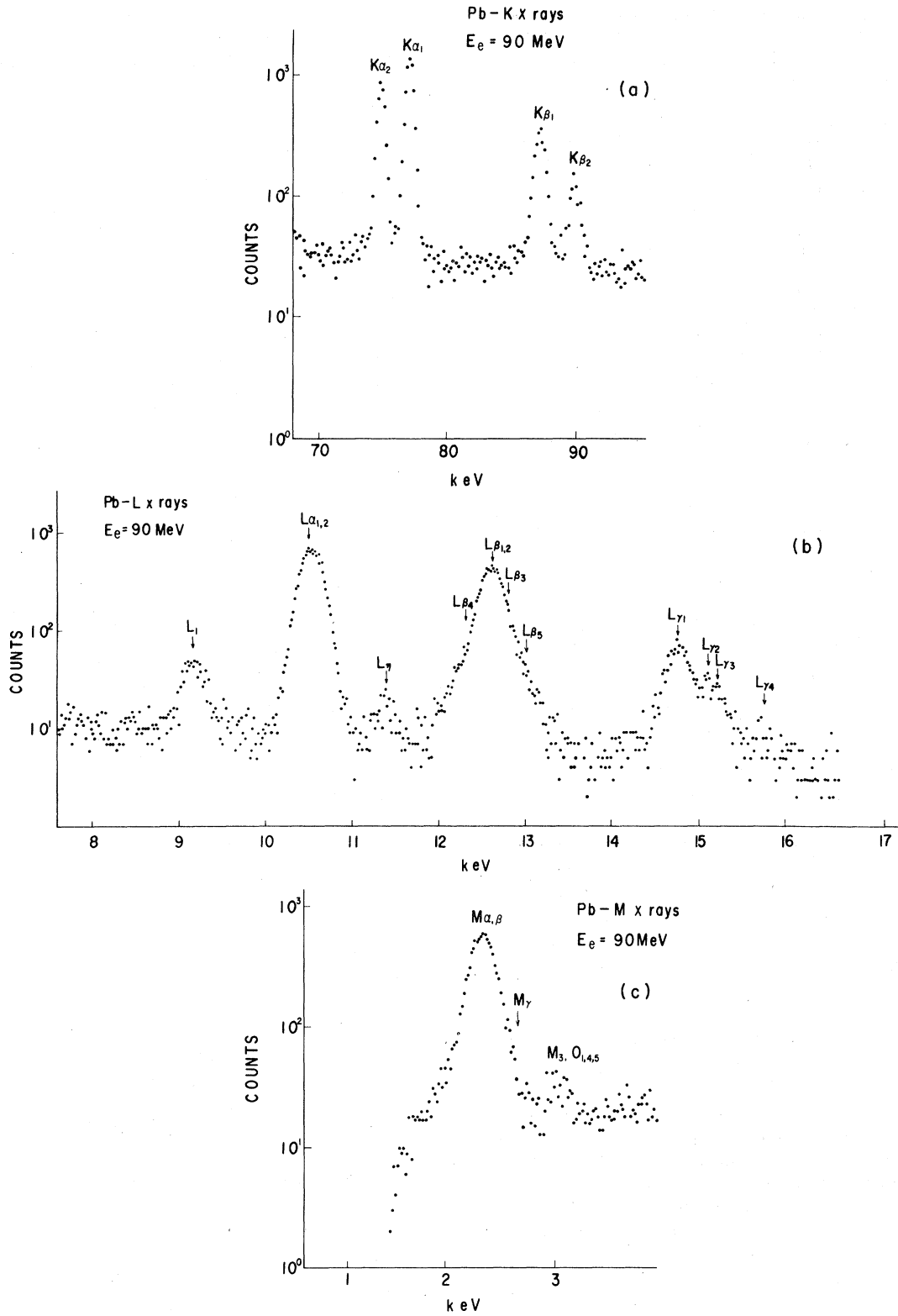


FIG. 2. (a) PbK x-ray spectrum obtained at  $E_e = 90 \text{ MeV}$  with the pure Ge detector. (b) PbL x-ray spectrum obtained at  $E_e = 90 \text{ MeV}$  with the Si(Li) detector. (c) PbM x-ray spectrum obtained at  $E_e = 90 \text{ MeV}$  with the Si(Li) detector. The lower energy part was cut off by the PHA bias.

TABLE II. *K*-shell ionization cross sections.

| Target | $E_e$ (MeV) | $\sigma^I$ (b)     | $\omega_K$ |
|--------|-------------|--------------------|------------|
| Al     | 150         | $2.84 \times 10^3$ | 0.0380     |
| Si     | 150         | $2.25 \times 10^3$ | 0.043      |
| Cl     | 270         | $1.27 \times 10^3$ | 0.0955     |
| Ca     | 70          | $8.89 \times 10^2$ | 0.163      |
|        | 150         | $9.08 \times 10^2$ |            |
|        | 270         | $1.05 \times 10^3$ |            |
| Cu     | 150         | $4.56 \times 10^2$ | 0.443      |
| Zn     | 150         | $3.96 \times 10^2$ | 0.479      |
| Se     | 70          | $2.69 \times 10^2$ | 0.596      |
|        | 150         | $2.74 \times 10^2$ |            |
| Y      | 70          | $1.89 \times 10^2$ | 0.711      |
|        | 150         | $1.87 \times 10^2$ |            |
|        | 270         | $2.05 \times 10^2$ |            |
| Mo     | 90          | $1.48 \times 10^2$ | 0.764      |
| Pd     | 90          | $1.16 \times 10^2$ | 0.819      |
|        | 250         | $1.23 \times 10^2$ |            |
| In     | 150         | $1.28 \times 10^2$ | 0.850      |
| Sn     | 150         | $1.11 \times 10^2$ | 0.859      |
| Ba     | 70          | $7.64 \times 10^1$ | 0.901      |
|        | 90          | $6.86 \times 10^1$ |            |
|        | 150         | $7.76 \times 10^1$ |            |
|        | 270         | $8.95 \times 10^1$ |            |
| Sm     | 90          | $5.36 \times 10^1$ | 0.928      |
| Ho     | 90          | $3.79 \times 10^1$ | 0.943      |
| Au     | 90          | $2.85 \times 10^1$ | 0.964      |
| Pb     | 90          | $2.26 \times 10^1$ | 0.972      |
| Bi     | 90          | $2.14 \times 10^1$ | 0.970      |
| U      | 90          | $1.80 \times 10^1$ | 0.970      |

\* Al, Si, Cl, and Ca—and 10% for heavier elements—Au, Pb, Bi, and U. These errors for the *L*- and *M*-shell ionization cross sections are 12 and 15%, respectively. These values were obtained by taking into account (1) uncertainties of detector efficiency of 5, 7, and 10% for the *K*-, *L*-, and *M*-shell x rays, respectively, (2) statistical uncertainties of 2, 3, and 4% for the *K*-, *L*-, *M*-shell x rays, respectively, (3) those for target thickness of 8–10%, and (4) uncertainty of geometrical factor of 5%. Large errors of 40% for lighter elements come from large absorption correction in the path because of the low x-ray energies and also from the large uncertainty of detector efficiency for these x rays.

As for theories which are applicable for inner-shell ionizations by ultrarelativistic electron impact, Davidović and Moiseiwitsch<sup>9</sup> have done PWBA calculations and Kolbenstvedt<sup>2</sup> has done calculations by the impact parameter method. Predictions from these theories are compared with the present experimental results on *K*-shell ionization at incident electron energy  $E_e = 90$  and 150 MeV in Fig. 3. As seen in this figure, the PWBA calculation gives good agreement with experimental results. The revised Kolbenstvedt theory, taking in-

TABLE III. *L*-shell ionization cross sections.

| Target | $E_e$ (MeV) | $\sigma^I$ (b)     | $\tilde{\omega}_L$ |
|--------|-------------|--------------------|--------------------|
| Pd     | 90          | $4.23 \times 10^3$ | 0.0559             |
|        | 250         | $4.71 \times 10^3$ |                    |
| In     | 150         | $4.95 \times 10^3$ | 0.0557             |
| Sn     | 90          | $3.52 \times 10^3$ | 0.0596             |
|        | 150         | $4.38 \times 10^3$ |                    |
|        | 250         | $3.30 \times 10^3$ |                    |
| Ba     | 90          | $2.48 \times 10^3$ | 0.0940             |
|        | 150         | $2.87 \times 10^3$ |                    |
|        | 250         | $2.76 \times 10^3$ |                    |
| Ho     | 90          | $1.25 \times 10^3$ | 0.213              |
| Au     | 150         | $9.69 \times 10^2$ | 0.349              |
| Pb     | 90          | $7.97 \times 10^2$ | 0.342              |
|        | 150         | $1.00 \times 10^3$ |                    |
|        | 250         | $8.56 \times 10^2$ |                    |
| Bi     | 90          | $6.55 \times 10^2$ | 0.409              |
|        | 150         | $8.01 \times 10^2$ |                    |
|        | 250         | $7.81 \times 10^2$ |                    |
| U      | 90          | $4.42 \times 10^2$ | 0.592              |

to account the screening number, also gives good agreements with experimental results. Since the Kolbenstvedt theory gives a clear physical picture on the mechanism of inner-shell ionization, our discussion will be mainly based on this theory.

The *L*-shell ionization cross sections are shown in Fig. 4(a), 4(b), and 4(c) for  $E_e = 90$ , 150, and 250 MeV, respectively. The results obtained by Middleman *et al.* are also shown. The solid lines in these figures were calculated from the Kolbenstvedt theory by using the photoeffect cross sections for the *L* shell given by Hall<sup>4</sup> instead of those for the *K* shell in the Kolbenstvedt calculation.

The results on *M*-shell ionizations for two heavy elements, Bi and Pb, are shown in Fig. 5. Here the solid curves were also obtained from the Kolbenstvedt theory using the photoeffect cross section for the *M* shell given by Hall. Here again good agreement is obtained between the experimental results and the calculation.

Though the Kolbenstvedt theory gives fairly good agreement with the experimental results on *K*-, *L*-, and *M*-shell ionization cross sections as de-

TABLE IV. *M*-shell ionization cross sections.

| Target | $E_e$ (MeV) | $\sigma^I$ (b)     | $\tilde{\omega}_M$ |
|--------|-------------|--------------------|--------------------|
| Pb     | 90          | $1.08 \times 10^4$ | 0.029              |
|        | 250         | $1.16 \times 10^4$ |                    |
| Bi     | 90          | $9.64 \times 10^3$ | 0.035              |
|        | 250         | $1.17 \times 10^4$ |                    |

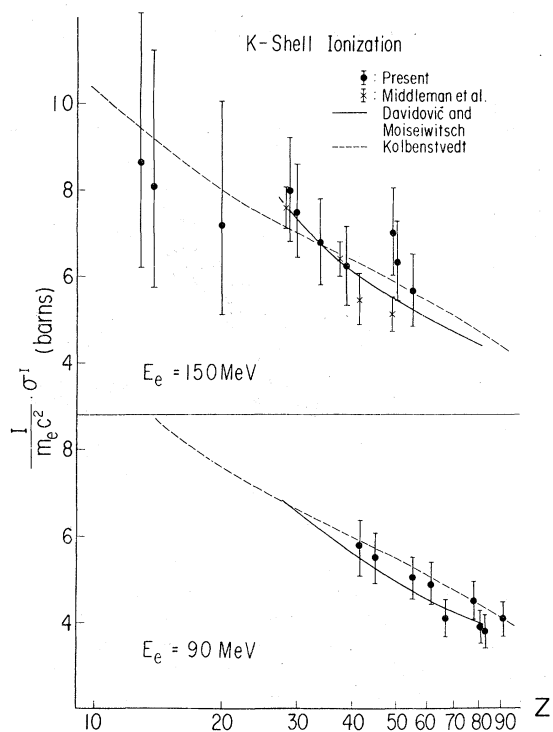


FIG. 3. *K*-shell ionization cross sections obtained at  $E_e = 90$  and  $150$  MeV are compared with the predictions from the revised Kolbenstvedt theory and from the PWBA calculation of Davidović and Moiseiwitsch. The results of Middleman *et al.* are taken from Ref. 1.

scribed above, it must be noted that there is ambiguity in the values of photoeffect cross section used in estimating the ionization cross section for distant collisions. The main contribution to the inner-shell ionization by distant collisions comes from the photoeffect cross section in the region just above the absorption edge, where Hall's formula<sup>4</sup> gives values fairly larger than experimental values.<sup>12</sup> For example, the photoeffect cross sections given by Hall are about twice the experimental values for the Al *K* shell, and as the atomic number increases the ratio of theoretical to experimental values gradually decreases, reaching about unity at the U *K* shell. The ratios for U *L* and *M* shells are 3 and 6, respectively. Therefore, if the experimental photoeffect cross sections were used in the theoretical estimation described above, the predicted inner-shell ionization cross sections would become fairly smaller than the experimental values. Nevertheless, it can be said that the ionization cross sections using the photoeffect cross sections of Hall give good agreement with the experimental ionization cross sections for the *L* and *M* shells as well as for the *K* shell. Although reasons for this in-

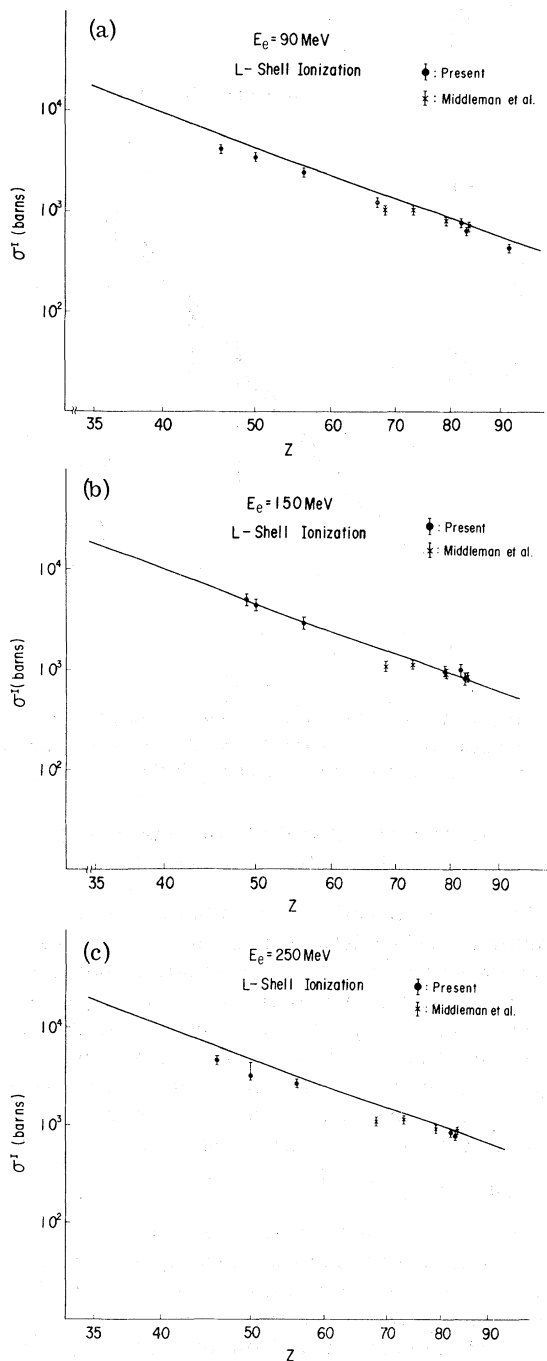


FIG. 4. (a) *L*-shell ionization cross sections measured at  $E_e = 90$  MeV as a function of atomic number. The solid line was estimated from the Kolbenstvedt theory. (b) Same as in (a), except for  $E_e = 150$  MeV. (c) Same as in (a), except for  $E_e = 250$  MeV.

consistency are not clear at the moment, it may be due to the difference between the real photoeffect and the virtual photoeffect used in the impact-parameter method.

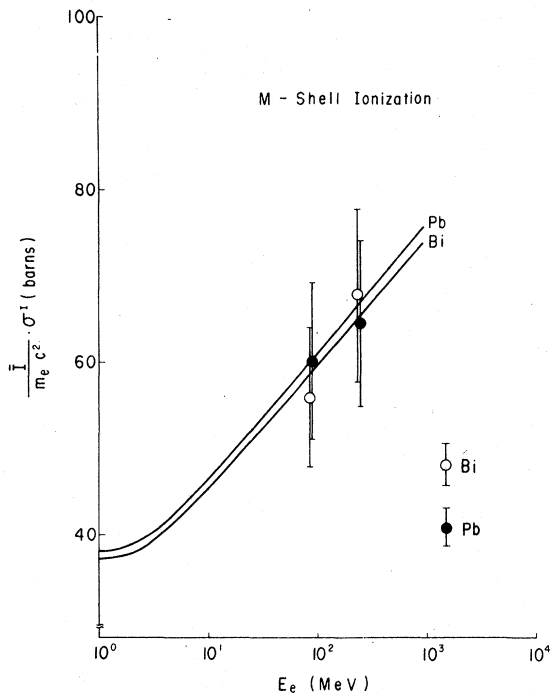


FIG. 5. *M*-shell ionization cross sections for Bi and Pb measured at  $E_e = 90$  and 250 MeV. The solid curves were estimated from the Kolbenstvedt theory.

#### IV. SCALED REPRESENTATIONS OF K-SHELL IONIZATION CROSS SECTIONS

Pessa and Newell<sup>13</sup> have given the correction factor for relativistic effects on inner-shell ionization cross section and obtained fairly good agreement with experimental results over the impact energy range  $3 \leq E_e/I \leq 25$ , where  $E_e$  is the incident electron energy and  $I$  is the ionization energy. Although the impact energy in the present experiment is much higher than the energy mentioned above, their calculations suggest a scaling law

$$I\sigma^I \propto \ln(E_e/I), \quad (2)$$

where  $\sigma^I$  is the ionization cross section.

Figure 6 shows this representation together with other experimental results. Here the experimental points are rather scattered and not so well scaled. Theoretical predictions from the revised Kolbenstvedt theory and the PWBA calculation by Davidović and Moiseiwitsch are shown by the dotted and the solid curves, respectively. Good agreement between the two theories and the experimental results is seen in this figure. Next,  $I\sigma^I$  versus  $E_e/I^2$  is plotted in Fig. 7, where the division of  $E_e/I$  by  $I$  means the displacement of experimental points for heavier elements in Fig. 6 to the left side. The scaling is much improved except for the results on Ni obtained by Dangerfield and

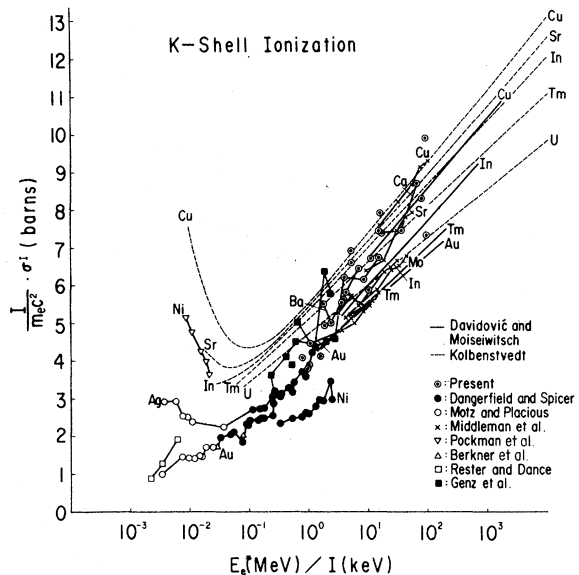


FIG. 6. Scaled representation following the Pessa-Newell theory. Dotted curves show the revised Kolbenstvedt theory; solid curves are from the Davidović and Moiseiwitsch theory. Experimental results other than the present ones are taken from the papers of Dangerfield and Spicer (Ref. 3), Motz and Placious (Ref. 14), Middleman *et al.* (Ref. 1), Pockman *et al.* (Ref. 15), Berkner *et al.* (Ref. 16), Rester and Dance (Ref. 17), and Genz *et al.* (Ref. 7).

Spicer.<sup>3</sup>

Since the revised Kolbenstvedt theory agrees well with the experimental results as seen in Figs. 3 and 6, we tried to deduce a scaling law

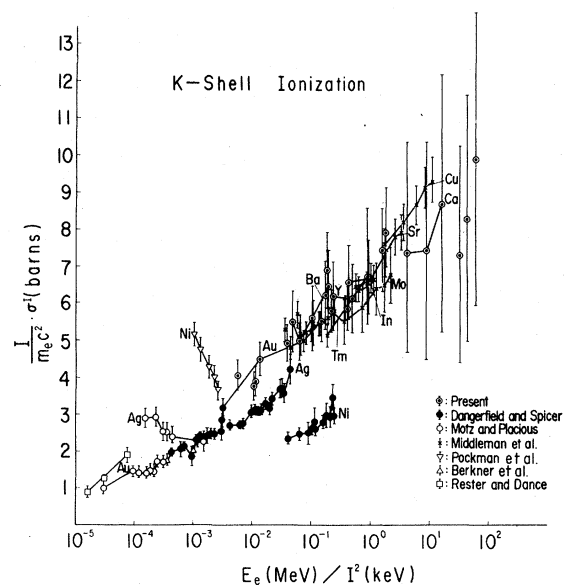


FIG. 7. Scaled representation in plots of  $I\sigma^I/m_e c^2$  versus  $E_e/I^2$ .

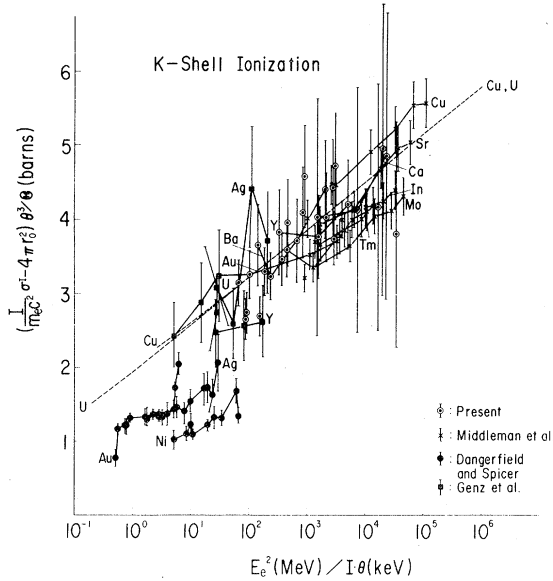


FIG. 8. Scaled representation following the revised Kolbenstvedt theory in the ultrarelativistic energy region.

from this theory. Assuming  $E_e \gg m_e c^2 = 0.511$  MeV ( $m_e$  being the electron rest mass), i.e., in the ultrarelativistic energy region, the revised Kolbenstvedt theory gives the following relation:

$$(\sigma^I - \sigma_0) I_{ob} \theta^3 / \Theta = f(E_e^2 / I_{ob} \theta) \quad (3)$$

with

$$\sigma_0 = 4\pi r_0^2 m_e c^2 / I_{ob} \quad \text{and} \quad \Theta = 1 - \frac{16}{13}(1 - \theta),$$

where  $I_{ob}$  is the observed ionization energy,  $\theta$  is the screening number,  $r_0$  is the classical electron radius, and  $\sigma_0$  is the ionization cross section for close collisions. Thus, by subtracting out the constant ionization cross section for close collisions, the relativistic increase of the cross section for distant collisions can theoretically be well scaled. Figure 8 shows the plot of experimental results following Eq. (3); the dotted line is the scaled prediction for all elements from the revised Kolbenstvedt theory. It must be noted that the scale of the ordinate is enlarged in comparison with that of Fig. 7. It is concluded from this figure that the experimental results can be well scaled and give good agreement with the theory, except those data of Dangerfield and Spicer, which show a discontinuity in relation to other measure-

ments on Ag and Au. It is unlikely that such an anomalous behavior might occur in the energy region 20–70 MeV. New measurements in this energy region would be desirable.

The theoretical line in Fig. 8 is expressed by

$$\frac{(\sigma_{th}^I - \sigma_0) I_{ob} \theta^3}{\Theta} \approx 144 \ln \frac{E_e^2}{I_{ob} \theta} + 1052 \text{ (barns)}$$

( $E_e$  in MeV,  $I_{ob}$  in keV), and the experimental points are fitted with  $\chi^2$  minimum by

$$\frac{(\sigma_{ex}^I - \sigma_0) I_{ob} \theta^3}{\Theta} \approx 129 \ln \frac{E_e^2}{I_{ob} \theta} + 1017 \text{ (barns)},$$

where  $\sigma_{th}^I$  and  $\sigma_{ex}^I$  are the theoretical and experimental ionization cross sections, respectively. Both lines coincide with each other within an experimental error of 10%.

## V. SUMMARY

$K$ -,  $L$ -, and  $M$ -shell ionization cross sections by electron impact have been measured over the energy range 70–270 MeV and the results on  $K$ -shell ionization compared with predictions from the revised Kolbenstvedt theory and from the PWBA calculations of Davidović and Moiseiwitsch. Good agreement is obtained between the experiment and the theories.

The measured  $L$ - and  $M$ -shell ionization cross sections were also compared with the Kolbenstvedt theory where the photoeffect cross sections for these shells were used, and it was found that this theory can give a good fit to the experimental results, although there is ambiguity in the values of the photoeffect cross section used in estimating the ionization cross section for distant collisions.

The  $K$ -shell ionization cross sections, together with other experimental results, were shown in scaled representations. In particular, a new scaling law for an ultrarelativistic energy region was derived from the revised Kolbenstvedt theory; it gives good agreement with the experimental results except those obtained by Dangerfield and Spicer in the region 20–70 MeV.

## ACKNOWLEDGMENTS

The authors would like to express their sincere gratitude to the staff of Laboratory of Nuclear Science for the operation of the accelerator during the course of this experiment.



- \*Now at Health Physics Department, National Tsing Hua University, Hsinchu, Taiwan, China.
- <sup>1</sup>L. M. Middleman, R. L. Ford, and R. Hofstadter, *Phys. Rev. A* **2**, 1429 (1970).
- <sup>2</sup>H. Kolbenstvedt, *J. Appl. Phys.* **38**, 4785 (1967). See also Ref. 1.
- <sup>3</sup>G. R. Dangerfield and B. M. Spicer, *J. Phys. B* **8**, 1744 (1975).
- <sup>4</sup>H. Hall, *Rev. Mod. Phys.* **8**, 358 (1936).
- <sup>5</sup>R. D. Schmickley and R. H. Pratt, *Phys. Rev.* **164**, 104 (1967).
- <sup>6</sup>G. R. Dangerfield, *Phys. Lett.* **46A**, 19 (1973).
- <sup>7</sup>H. Genz, D. H. H. Hoffmann, A. Richter, and E. Spamer, *Abstracts of Contributed Papers, Second International Conference on Inner-Shell Ionization Phenomena*, Freiburg, p. 229 (1976).
- <sup>8</sup>H. Tawara, K. Ishii, S. Morita, H. Saito, M. Oyamada, H. Kaji, and T. C. Chu, *Phys. Lett.* **54A**, 171 (1975).
- <sup>9</sup>D. M. Davidović and B. L. Moiseiwitsch, *J. Phys. B* **8**, 947 (1975).
- <sup>10</sup>H. Tawara, K. Ishii, S. Morita, H. Kaji, C. H. Hsu, and T. Shiokawa, *Phys. Rev. A* **9**, 1617 (1974). K. Ishii, S. Morita, H. Tawara, H. Kaji, and T. Shiokawa, *Phys. Rev. A* **10**, 774 (1974).
- <sup>11</sup>W. Bambyneck, B. Crasemann, R. W. Fink, H. U. Freund, H. Mark, C. D. Swift, R. E. Price, and P. Venugopala Rao, *Rev. Mod. Phys.* **44**, 716 (1972).
- <sup>12</sup>R. H. Pratt, A. Ron, and H. K. Tseng, *Rev. Mod. Phys.* **45**, 273 (1973).
- <sup>13</sup>V. M. Pessa and W. R. Newell, *Phys. Scr.* **3**, 165 (1971).
- <sup>14</sup>J. W. Motz and R. C. Placious, *Phys. Rev.* **136**, A662 (1964).
- <sup>15</sup>L. T. Pockman, D. L. Webster, P. Kirkpatrick, and K. Harworth, *Phys. Rev.* **71**, 330 (1947).
- <sup>16</sup>K. H. Berkner, S. N. Kaplan, R. V. Pyle, *Bull. Am. Phys. Soc.* **15**, 786 (1970).
- <sup>17</sup>D. H. Rester and W. E. Dance, *Phys. Rev.* **152**, 1 (1966).